JGR Atmospheres

RESEARCH ARTICLE
10.1029/2019JD030682

The Influence of Tropical Cyclones on Circulation, Moisture Transport, and Snow Accumulation at Kilimanjaro During the 2006–2007 Season

E. Collier[1], **T. Sauter**[1], **T. Mölg**[1], **and D. Hardy**[2]

[1]Climate System Research Group, Institute of Geography, Friedrich-Alexander University Erlangen-Nürnberg, Erlangen, Germany, [2]Department of Geosciences, Morrill Science Center, University of Massachusetts Amherst, Amherst, MA, USA

Key Points:
- Tropical cyclones in the southwest Indian Ocean impact high-elevation atmospheric conditions on Kilimanjaro
- They influence regional moisture and precipitation through direct storm circulations and indirectly triggered westerlies
- Single-day observed snowfall on the glaciers during two storms each exceeded ~5% of the average annual total snow accumulation

Supporting Information:
- Supporting Information S1

Correspondence to:
E. Collier,
emily.collier@fau.de

Citation:
Collier, E., Sauter, T., Mölg, T., & Hardy, D. (2019). The influence of tropical cyclones on circulation, moisture transport, and snow accumulation at Kilimanjaro during the 2006–2007 season. *Journal of Geophysical Research: Atmospheres*, *124*, 6919–6928. https://doi.org/10.1029/2019JD030682

Received 21 MAR 2019
Accepted 25 MAY 2019
Accepted article online 10 JUN 2019
Published online 4 JUL 2019

Abstract Tropical cyclones represent an important component of intraseasonal atmospheric variability in the southwest Indian Ocean, and their landfall can be devastating to coastal communities. However, little is known about their impact on precipitation in the high-elevation regions of East Africa. Here we combine in situ measurements from the summit of Kilimanjaro and subkilometer atmospheric modeling of the region to investigate the impact of these storms during the 2006–2007 cyclone season, which was characterized by anomalously positive snow accumulation at the summit coinciding with cyclone activity. Observations indicate that two storms are associated with snowfall amounts exceeding 10 cm per day, an amount representing ~5% of the observed average annual total. Numerical simulations show that some tropical cyclones transport moisture directly to the region while others induce moisture transport from the continental interior. Our study suggests that these synoptic-scale phenomena have the potential to complicate the extraction of climate signals from glaciers.

Plain Language Summary Tropical cyclones in the southwest Indian Ocean have a devastating impact on the coastal populations of East Africa and Madagascar when they make landfall. However, very little is known about their impact on the high-mountain areas of East Africa and on the small glaciers in those regions. Focusing on Kilimanjaro, we show that these storms coincide with some of the largest measured daily snowfall amounts at the summit, with some transporting moisture to the region through storm winds and others triggering moisture transport from the continental interior. The magnitude of the snowfall that occurs during two tropical cyclones means that these storms, which typically only last for a few days, can be relevant for understanding climate signals recorded by glaciers (e.g., ice cores).

1. Introduction

Tropical cyclones (TCs) represent an important component of intraseasonal atmospheric variability in the southwest Indian Ocean (SWIO), with an average of 12 to 13 TCs forming in this region each year. The cyclone season in the SWIO lasts from November to April, during which time 85% of storms occur, with peak activity concentrated during the months of January and February (e.g., Ho et al., 2006; Mavume et al., 2009). Landfall of TCs is associated with substantial damage to infrastructure and agriculture, and with significant loss of life in the coastal countries of East Africa, in particular Mozambique, and the island of Madagascar (e.g., Chang-Seng & Jury, 2010; Fitchett & Grab, 2014; Matyas & Silva, 2013).

Variations in TC activity in the SWIO have been linked to several modes of interannual variability. The El Niño–Southern Oscillation (ENSO) is associated with a westward shift of cyclogenesis (enhanced TC activity west of ~80°E) but a reduction in the total number of cyclones during El Niño compared with neutral and La Niña conditions (Astier et al., 2015; e.g., Ho et al., 2006; Kuleshov et al., 2008), which may be related to meridional displacements of the subtropical jet that alter wind shear in TC genesis regions (Astier et al., 2015). The Indian Ocean Subtropical Dipole (IOSD) and its interactions with ENSO also impact cyclone tracks in this region (Ash & Matyas, 2012; Fitchett & Grab, 2014), with enhanced westward and southwestward components during positive IOSD and neutral ENSO conditions (Ash & Matyas, 2012).

At intraseasonal time scales, the Madden-Julian Oscillation (MJO; Madden & Julian, 1994) is an important modulator of tropical convection and cyclogenesis, whose activity is often divided into eight phases (Wheeler & Hendon, 2004). In the SWIO, TC activity is enhanced as the center of convection associated with this mode traverses eastward over the Indian Ocean and Maritime Continent (phases 2 to 5). Conversely, TCs are

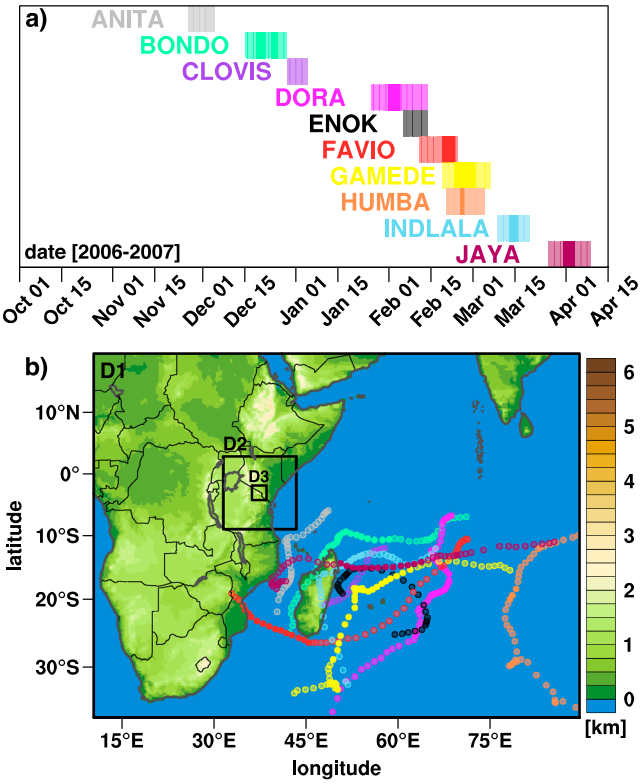

Figure 1. (a) A summary of TC activity in the SWIO between November 2006 and April 2007, with colored polygons indicating the lifetime of each storm (*y* axis is dimensionless). Fully opaque shading delineates periods with central pressures below 970 hPa, a threshold for severe TCs in the Southern Hemisphere (Kuleshov, 2012). (b) The extent and modeled topography of D1, and the best-track data for each TC. The same color of polygons and markers is used for each storm in all figures.

suppressed when convection is enhanced over the western Pacific and Western Hemisphere (phases 6 to 7 and 8 to 1; Bessafi & Wheeler, 2006; e.g., Ho et al., 2006; Klotzbach, 2014; Ramsay et al., 2012).

Although the relevance of TCs for coastal populations in East Africa is well established, their influence on atmospheric conditions in the equatorial high mountains remains unknown but may influence the signal of atmospheric variability recorded by the glaciers in these regions. In this paper, we combine high-elevation observations and subkilometer atmospheric modeling to investigate the impact of these synoptic-scale phenomena on Kilimanjaro during the 2006–2007 cyclone season. We focus on a single cyclone season to gain a process-based understanding of their impact, and on this year in particular because it was characterized by anomalously high snowfall on the glaciers at the summit (e.g., Mölg, Cullen, et al., 2009) coinciding with TC activity (Collier et al., 2018), and by severe flooding events in northern Tanzania that caused great loss of life and property damage (Kijazi & Reason, 2009).

2. Data, Methods, and Model Evaluation

Data about TC activity were obtained from the Southern Hemisphere Tropical Cyclone (SHTC) Data Portal (http://www.bom.gov.au/cyclone/history/tracks). These data show that the 2006–2007 cyclone season lasted from late November 2006 until mid-April 2007, with a total of 10 cyclones (Figure 1a and Table S1). TCs Anita, Clovis, and Enok were classified as tropical storms (maximum sustained 10-min near-surface wind speeds of 63 to 117 km/hr), while Bondo, Dora, Favio, Gamede, Indlala, and Jaya developed into intense TCs (166 to 212 km/hr). Humba reached TC status (118 to 165 km/hr) but remained more than 5,000 km away from Kilimanjaro during its lifetime; therefore, we neglected this storm in individual analyses. The study period was characterized by weakly positive ENSO conditions in the tropical Pacific and a positive Indian Ocean Zonal Mode event (Collier et al., 2018). The IOSD was also strongly positive in boreal winter and spring (http://www.jamstec.go.jp/res/ress/behera/iosdindex.html). Although the total number of storms in this year was below average, the total number of days that a TC was present in the SWIO was the third highest on record between 1981 and 2013 (Astier et al., 2015), indicating their persistence in the basin.

Observational data were taken from two automated weather stations (AWS) installed at the summit of Kilimanjaro: (i) AWS 1, which is located on the Northern Icefield (37.34648°E, 3.05933°S) at an elevation of 5,775 m and has been operational since 2000, and (ii) AWS 3, which is located on the upper part of Kersten Glacier on the southern slopes (37.354°E, 3.078°S) at an elevation of 5,873 m and whose data are available from 2005 to 2013 (Figure S1). Additional information is provided in Text S1 in the supporting information (Cullen et al., 2013; Mölg et al., 2008; Mölg, Chiang, et al., 2009; Mölg & Hardy, 2004). To quantify the importance of TCs for precipitation in the lowlands surrounding Kilimanjaro, we also used data from the Tropical Rainfall Measuring Mission (TRMM) (e.g., Huffman et al., 2007) 3B43 product at a horizontal resolution of 0.25° and on a daily time scale, area averaged over the same spatial extent as D3 (cf. Figure 1b). Mölg, Chiang, et al. (2009) showed that this product compares well with low-altitude rain gauge data near the mountain. Data over the period of January 2000 to December 2017 were used for computing 95th percentiles of daily precipitation for each month, considering only days with nonzero values after area averaging.

We performed simulations with the advanced research Weather Research and Forecasting (WRF) model 3.9.1.1, configured with three one-way nested domains of 20-km, 4-km, and 800-m grid spacing centered over Kilimanjaro (D1–3; Figure 1b). We employed the same model configuration as Collier et al. (2018) including analysis nudging in D1 to constrain the large-scale circulation, as this study optimized the

model for this region and evaluated its performance in detail. However, we enlarged the domains to encompass TC trajectories. More information about the atmospheric modeling is in Text S2 in the supporting information (Banzon et al., 2013; Dee et al., 2011; Mölg & Kaser, 2011; Reynolds et al., 2007). For the main simulation, we ran WRF with the aforementioned configuration continuously from 23 September 2006 to 15 April 2007, discarding the first eight days as spin-up time and allowing nearly two months of simulation before the first TC formed. A comparison of daily mean atmospheric variables from the AWSs and the results from D3 indicates that the model has strong but compensating biases in the simulated radiation fields and underestimates the highest observed daily precipitation events. However, the model represents variability in surface pressure, incoming longwave radiation, atmospheric humidity, wind speed, and wind direction well (see Text S2 and Figure S2). Recent work has also shown that WRF can capture the fundamental physical processes underlying moisture transport and precipitation formation elucidated by detailed observational campaigns despite errors in the magnitude due to the model's representation of microphysical processes (Wang & Kirshbaum, 2015). We therefore used the model results for understanding the atmospheric dynamics and mesoscale flow patterns near the mountain, and on the observations for assessing the impact on snow accumulation on the glaciers.

To evaluate the influence of the storms relative to a "null" scenario, we performed three additional sensitivity simulations with WRF for each storm. Each simulation covered the lifetime of each storm, plus one day of spin-up. For TC "pairs" Bondo & Clovis, Dora & Enok, and Gamede & Humba, the model was run for their combined life spans due to temporal overlap. The simulations employed the same configuration as the long integration but varied in their forcing strategy: WRFS used analysis nudging in D1, as in the main simulation; WRFS_NN neglected nudging; and WRFS_NN_SST neglected nudging and limited sea surface temperature at 26 °C, below the commonly cited threshold of 26.5 °C for TC development (e.g., Wallace & Hobbs, 2006). The initial conditions for WRFS_NN_SST were also modified to remove the developing vortex using the built-in scheme ("*tc.exe*"). These two changes were sufficient to suppress TCs in all cases, thereby elucidating the circulation and moisture transport patterns that arise due to the presence of the storms.

To evaluate the representation of TCs in D1, we used the National Oceanic and Atmospheric Administration Geophysical Fluid Dynamics Laboratory vortex tracking scheme version 3.9a (Biswas et al., 2018), which estimates the position and intensity of a storm based on sea level pressure and lower tropospheric winds, relative vorticity, and geopotential height. Compared with best track data from the SHTC, the model underestimates storm intensity (Figure S3), overestimating the minimum pressure by more than 25 hPa for all storms except for TCs Anita, Enok, Humba, and Gamede. For all intense TCs except Gamede (Bondo, Dora, Favio, Indlala, and Jaya) the difference between observed and simulated minimum central pressure exceeds 60 hPa. For TCs Anita and Indlala, the period over which the cyclone is detectable by the tracking scheme is also shorter than the observed lifetime, as the simulated storms dissipate too quickly after making landfall on Mozambique (erroneously) and Madagascar, respectively. However, the trajectory and therefore the angle of approach and distance from our study area are in general well captured.

The strengths and weaknesses of the model's representation of TC activity are directly related to the use of grid analysis nudging in D1: applying the vortex tracker to the aforementioned sensitivity runs shows that the model predicts much deeper central pressures without nudging, in closer agreement with observations. The largest bias between simulated and observed minimum central pressure for all intense TCs except Gamede is halved (~30 hPa). Without nudging, the model also correctly differentiates between TC and intense TC status for all storms except Clovis, where the central pressure is 15 hPa too low and therefore below the threshold for intense TCs (Figure S4), and Enok, where the developing vortex merges with TC Dora prior to the best-track start date (not shown). The difference is consistent with nudging toward ERA-Interim data (see Text S2), whose spatial resolution of ~80 km is likely to be inadequate for representing intense TCs (Davis, 2018). However, without nudging errors in the storm trajectory, and therefore in the angle of approach and distance from Kilimanjaro, are greater. We therefore retained analysis nudging in our forcing approach, although the underestimation of storm intensity likely contributes to discrepancies between observed and simulated atmospheric conditions at the summit, such as the underestimation of the largest precipitation events (cf., Text S2), and an underestimation of the importance of these synoptic-scale events in our simulations.

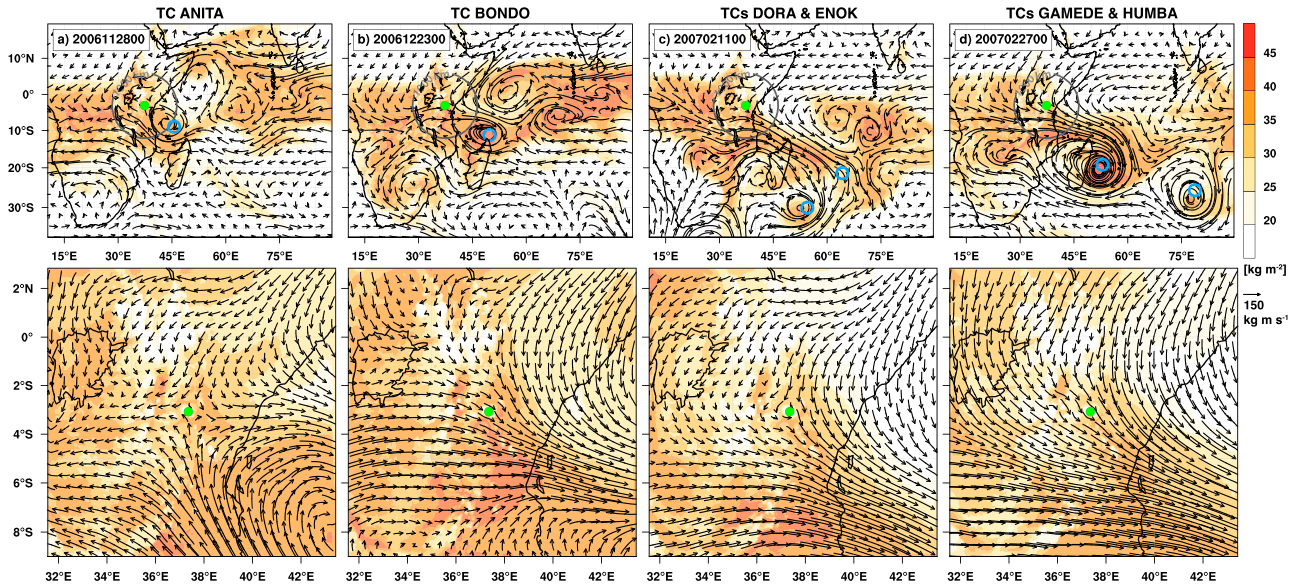

Figure 2. Daily mean specific humidity (shading) and moisture fluxes (black vectors) from the main WRF simulation vertically integrated between 900 and 500 hPa for D1 and D2 (top and bottom rows) for (a) Anita, (b) Bondo, (c) Dora & Enok, and (d) Gamede & Humba. The green circle shows the location of Kilimanjaro; the grey circle delineates a radius of 1,000 km around the mountain, and the blue circle indicates the best-track locations.

Finally, to assess moisture source regions, we computed back trajectories throughout the lifetime of each storm using the model LAGRANTO (Sprenger & Wernli, 2015) with data from D1. The trajectories were seeded at the locations of the two stations, which fall within the same grid cell in D1, as well as the center of this grid point and the three others with the highest topographic height representing Kilimanjaro, at altitudes ranging from 2,000 to 5,000 m in 500-m intervals. The trajectories were computed every 3 hr over 10 days. Back trajectory densities were computed from the normalized sum of the number of times a trajectory was present in each grid cell in D1.

3. Results and Discussion

The simulated low- to middle-tropospheric moisture transport to Kilimanjaro is northeasterly and easterly in boreal fall and spring, respectively (Figure S5). Superimposed on these background flow patterns, the atmospheric simulations indicate that TCs in this season influence regional moisture transport patterns in two ways, directly and indirectly (Figure 2). The first pattern is simulated when certain storms bring moisture directly to the region as they approach the East African coastline. Taking the time slice of 28 November 2006 during TC Anita as an example, the simulations show that southeasterly moisture fluxes arising from the cyclonic circulation impinge on Kilimanjaro (at ~850 hPa) and converge with monsoonal fluxes near the mountain (Figure 2a). Similar patterns are simulated during TCs Indlala and Jaya (not shown).

The second pattern is an "indirect" westerly moisture flux originating from the continental interior that develops when at least one intense TC approaches East Africa, and during this study period, often another storm is present or forming in the basin. Figures 2b–2d show three examples of this flow configuration for three times slices: (i) 23 December 2006 during TC Bondo, with TC Clovis forming around 67°E; (ii) 11 February 2007 during TCs Dora (55°E) and TS Enok (65°E), with TC Favio forming around 75°E; and (iii) 27 February 2007 during TCs Gamede and Humba. The westerly moisture flux extends meridionally from a northern boundary near Kilimanjaro another ~10–20° to the south, and zonally from the Atlantic to the northern tip of Madagascar or even further east, depending on the storm. The spatial pattern is consistent with observations of higher frequencies of strong low-level westerlies in boreal winter in the Madagascar channel (Moore, 2013). A vertical cross section reveals that this westerly flow extends throughout the lower troposphere, with peak transport between ~800 and 600 hPa (Figure S6), a layer whose moisture content exerts an important control on snowfall magnitudes at the summit (Mölg, Chiang, et al., 2009). The simulations also show that northwesterly lower level inflow from Uganda and southeastern Kenya brings moisture

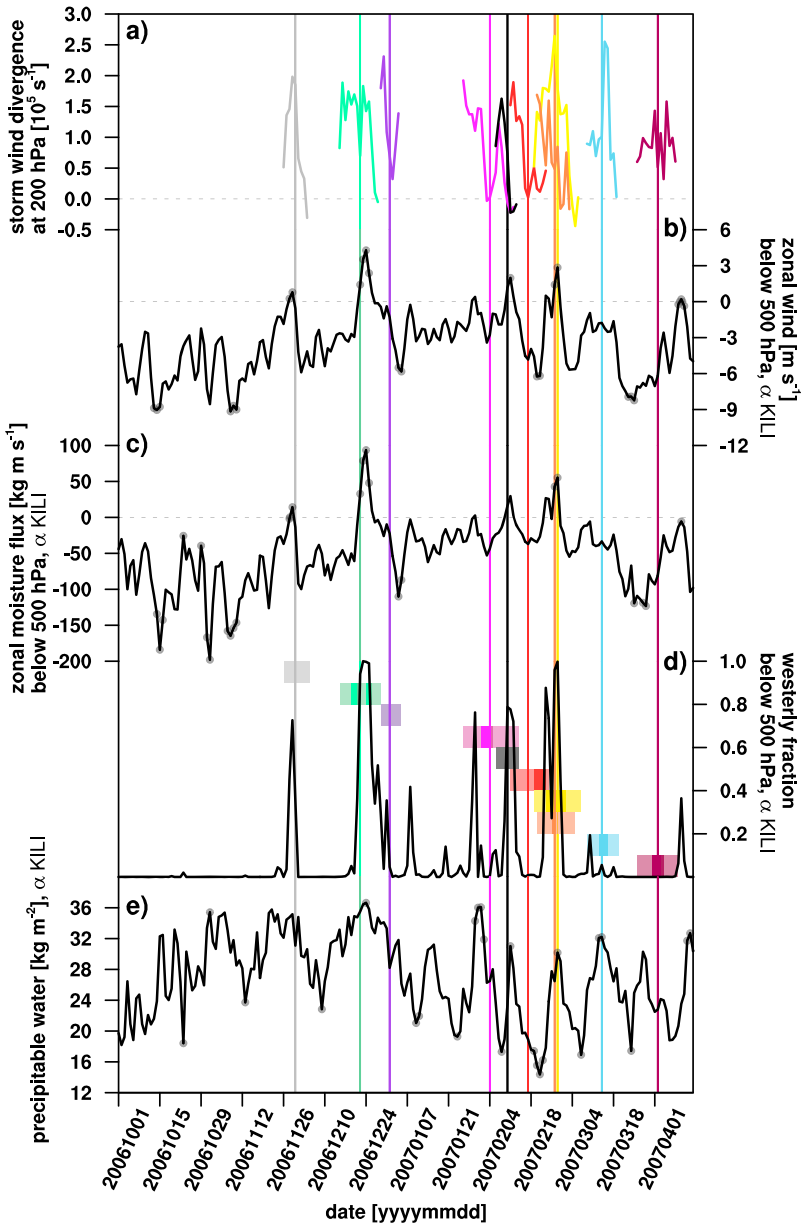

Figure 3. (a) Daily mean wind divergence at 200 hPa in D1, averaged in a 1,000-km-wide box around each storm over its lifetime. Daily mean zonal (b) wind and (c) moisture flux in D3, vertically averaged and integrated between 900 and 500 hPa, respectively, and spatially averaged over α_{KILI} (coordinates of AWS3 ± 0.4°). (d) The fraction of grid cells in α_{KILI} with a wind direction between 200° and 340°, computed using mean winds between 900 and 500 hPa. (e) Daily mean precipitable water averaged over α_{KILI} in D3. The data presented in all panels are from the main WRF simulation. Grey dots in (b)–(d) indicate days when the respective time series exceed ±1.5σ after being converted into standardized daily anomalies by subtracting the 45-day running mean.

to Kilimanjaro and, at times, converge upstream with monsoonal winds, a feature that has been identified in composite analysis of snowfall events at the summit during positive Indian Ocean Zonal Mode events (Chan et al., 2008).

Examination of the circulation dynamics indicates that upper tropospheric divergence, and the associated decrease in mean sea level pressure and resulting reversal of the simulated land-ocean pressure gradient (not shown), may drive the development of the westerly inflow when one or more intense TCs approach the East African coastline (Figure 3a). The advance of these storms toward East Africa coincides with the

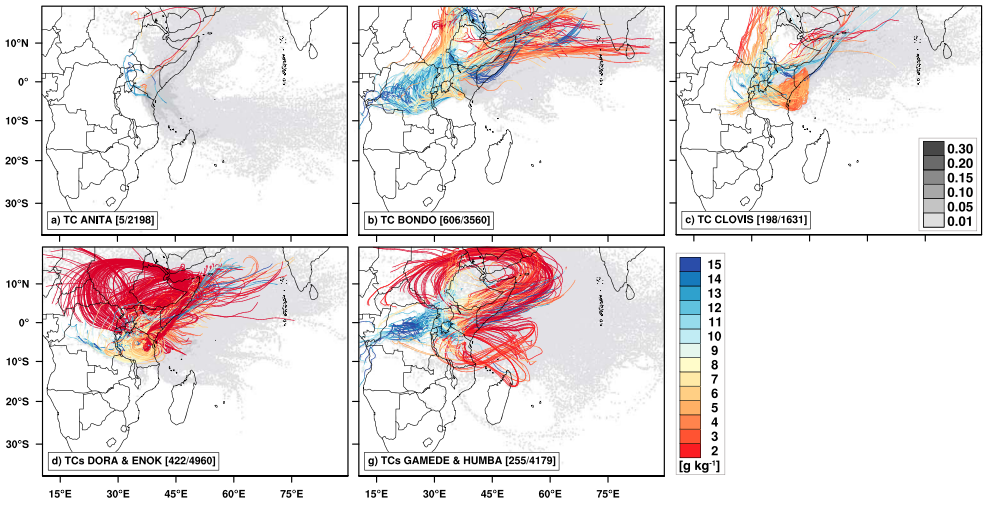

Figure 4. The back trajectory densities computed from the main WRF simulation for (a) Anita, (b) Bondo, (c) Clovis, (d) Dora & Enok, and (e) Gamede & Humba (grey shading). Westerly trajectories are defined as having at least one valid data point to the west of 35°E between 5°S and 5°N and are colored by specific humidity along the path. The numbers in brackets indicate the number of westerly trajectories compared with the total number. The results for Anita are representative of those for Indlala [2/2780] and Jaya [0/3859]. More than 75% of the westerly trajectories during Favio [47/3346] overlapped with the lifetimes of Dora & Enok and are not presented.

only periods when the mean zonal wind and moisture flux around Kilimanjaro are westerly, compared to a predominantly easterly regime over the simulation period (Figures 3b–3d; a higher westerly fraction during TC Anita reflects outflow from convergent north- and south-easterly winds, a feature that is also visible in the moisture fluxes in Figure 2a). The direction change is also observed in the AWS records (Figure S2). In total, the direction of moisture transport to Kilimanjaro is between 200 and 340° on 13 days during the study period: 29 November (convergent outflow), 22–26, and 28 December; 30 January; and 10–12 and 23–27 February, although the circulation feature persists a few days longer further south. The simulation indicates that these periods are associated with higher precipitable water in the region, in particular during the typically drier months of January and February (Figure 3e).

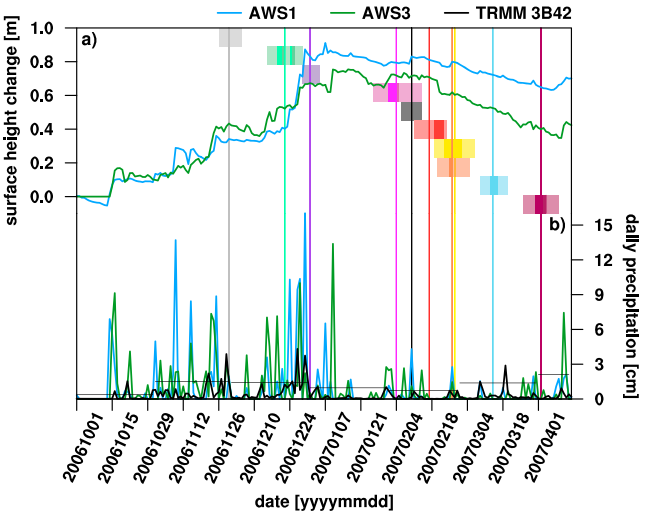

Figure 5. Observed daily (a) surface height change and (b) precipitation. Data from AWS1, AWS3, and TRMM are shown by the blue, green, and black curves. Black horizontal lines in (b) show the 95th percentile for each month from TRMM.

The back trajectory analysis shows that, although air parcels arriving at the mountain during storms predominantly originate from the background monsoonal circulation (Figure 4), during TC pairs Bondo & Clovis, Dora & Enok, and Gamede & Humba, more than 5% of all trajectories are westerly (defined as passing west of 35°E between 5°S and 5°N). The transport of moist air (on the order of 10 g/kg) from the continental interior and Congo Basin is particularly evident for the first and last storm pairs. Furthermore, air parcels moving along westerly trajectories often arrive at the mountain directly before large snowfall events are measured at the stations. This result is most pronounced for Bondo, when westerly trajectories comprise 53 and 82% of the total (n = 287) arriving on 23 and 24 December, respectively, before 10 cm of accumulation at AWS1 on the latter day (Figure 5). This single-day accumulation amount corresponds to ~5% of the average annual total at each of the stations. Similarly, 10 to 30% of valid trajectories ($104 < n < 282$) are westerly between 27 and 30 December, during which time three additional precipitation events of the same magnitude are measured at the stations. During January and February, the magnitude of observed precipitation associated with westerly proportions exceeding ~20% ($n \approx 275$) is on the order of 1 cm (e.g., 1–2 and 26–27 February). For comparison, the 90th percentile for daily snowfall during these months considering all days with nonzero

values on record is ~3.7 cm/day at each station. Therefore, while the Congo has been proposed as a source region for glaciers on Ruwenzori (Whittow, 1960), the simulations suggest that moisture from this region also contributes to high-elevation precipitation on Kilimanjaro when the westerly circulation is established.

The large snow accumulation at the AWSs during TCs Bondo & Clovis (cf. Figure 5) contribute to the short rains of 2006 being the most anomalously positive on record at both stations, with the snow cover extending from the summit down to ~4,500 m (Kaser et al., 2010). The unusually deep snowpack persisted for more than half a year, bridging the secondary dry season and insulating the glaciers from atmospheric energy sources and longwave emission by the surrounding dark ash surfaces, which has been proposed as a mechanism for initiating growth of the plateau glaciers on Kibo (Kaser et al., 2010). A corollary of our results is therefore that these extreme synoptic-scale events can have an important and previously unrecognized glaciological impact, which could be misinterpreted as being driven by an underlying influence acting on climatic time scales (e.g., interannual mode or climate trend). The TRMM data also show that all TCs except Favio and Jaya are associated with precipitation in the surrounding lowlands that reaches or exceeds monthly 95th percentiles (Figure 5b). The processes identified agree with Kijazi and Reason (2009), who found upper level divergence, cyclonic circulation near the coast, and moisture convergence over Tanzania contributed to the severe flooding events during the 2006 short rains using reanalysis data.

A number of previous studies have identified anomalous westerly winds across equatorial Africa and eastward moving convective systems as contributors to intraseasonal rainfall variability in East Africa (e.g., Davies et al., 1985; Mpeta & Jury, 2001; Mutai & Ward, 2000; Pohl & Camberlin, 2006; Sun et al., 1999). This circulation pattern has been attributed to the MJO (Mpeta & Jury, 2001; Mutai & Ward, 2000; Pohl & Camberlin, 2006), based largely on composite analysis of pentad data from atmospheric models and reanalyses, whose coarse spatial resolutions limit a realistic representation of TCs, in particular of intense storms for which a grid spacing of less than 0.25° is needed (Davis, 2018). Composite and pentad averaging, as well as temporal filtering (e.g., Pohl & Camberlin, 2006), may also have masked a potential contribution from TCs, as translational velocities are estimated to be ~200 km per day (Mavume et al., 2009). During our study period, there is no consistent temporal congruency between MJO phase and the development of the anomalous westerly circulation and moisture flux. Archived phase-space diagrams for the MJO from the Australian Bureau of Meteorology (http://www.bom.gov.au/climate/mjo) indicate that this oscillation may have contributed to the circulation dynamics during TCs Bondo & Clovis and Gamede & Humba, as the oscillation was in phases 3 to 5 (convective center over the Indian Ocean and Maritime Continent). However, during TCs Dora & Enok, the westerly moisture flux occurs independently of any significant regional enhancement or suppression of convection by the MJO, which was in phases 6 to 1 (convective center in the western Pacific and Western Hemisphere).

The hypothesized role of TCs in transporting moisture both indirectly and directly, as well as contributing to the development of the westerly circulation, is supported by the sensitivity simulations (Figures 6 and S7). When storm development is suppressed for the simulations of TCs Bondo & Clovis, Dora & Enok, and Gamede & Humba, the westerly moisture flux fails to develop for the former and is greatly weakened for the latter two storm pairs (Figures 6b and 6c). There is a correspondingly large simulated reduction in lower level humidity and precipitation over D3 (and at high elevations; not shown) for the first two storm pairs, although minimal changes in humidity and a slight increase in precipitation are simulated for the latter (Figures 6a and 6d). The remaining westerly fraction in D3 in the WRFS_NN_SST simulation of Dora & Enok and Gamede & Humba reflects the influence of a low-pressure system over the continental interior south of Kilimanjaro (visible in Figures 2c and 2d), which may act as a supporting factor. The closer proximity of this feature to the mountain in the WRFS_NN_SST simulation of the last storm pair (not shown) may contribute to the differing humidity and precipitation results compared with the other two pairs. In contrast, when nudging is not used, the model produces more intense TCs and enhanced westerly moisture transport and precipitation over D3 (Figure 6). Therefore, upper tropospheric divergence due to the presence of one or more intense TCs in the SWIO represents a plausible mechanism for triggering or enhancing the westerly circulation.

Suppression of TCs Anita and Indlala similarly produces simulated decreases in humidity and cumulative precipitation (Figure S7). However, stronger easterly moisture transport to Kilimanjaro occurs in the absence of TC Favio and toward the end of TC Jaya, which is associated with enhanced humidity at times

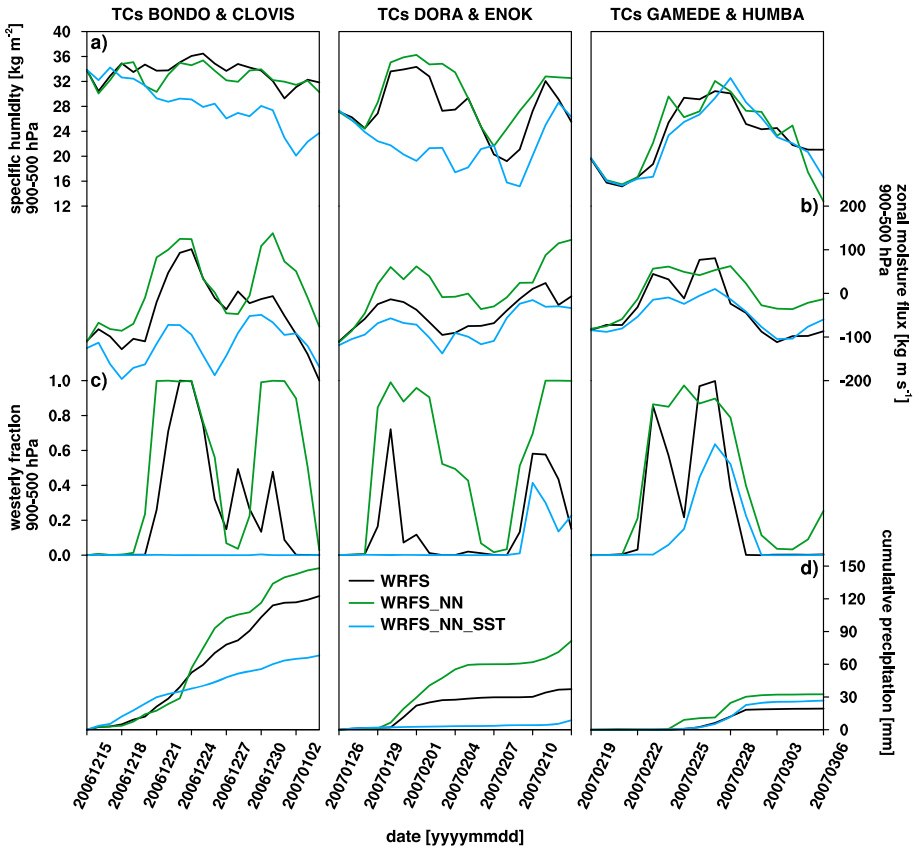

Figure 6. Daily mean (a) specific humidity and (b) zonal moisture flux, vertically integrated and averaged between 900 and 500 hPa, respectively, and (c) the total fraction of grid cells in α_{KILI} with a wind direction between 200° and 340°, computed using mean winds between 900 and 500 hPa. (d) Daily cumulative precipitation. All data are from the short sensitivity studies with WRF (see section 2) and were spatially averaged over WRF D3. Data from WRFS, WRFS_NN, and WRFS_NN_SST are shown by the black, green, and blue curves.

and increased total precipitation in WRFS_NN_SST compared with WRFS. Nonetheless, more intense simulated TCs in the WRFS_NN simulations are associated with greater cumulative precipitation in all cases (Figures 6 and S7). Therefore, in combination with the TRMM data (cf. Figure 5b), the sensitivity simulations indicate that TCs in this season are important not only for glaciers but also on a regional scale for agriculture, as crop yields are sensitive to moisture fluctuations (e.g., Barron et al., 2003); for water availability (Hemp, 2005); and for biological and ecological research of endemic fauna and flora (e.g., Hemp, 2006).

4. Conclusions and Outlook

A combination of subkilometer atmospheric modeling and observational records indicate that TC activity in the SWIO had an important influence on precipitation at Kilimanjaro, both at the summit and in the surrounding lowlands, during the 2006–2007 cyclone season. Our analysis indicates that their impact was manifested through direct moisture transport by certain storms, while other—or multiple—intense TCs contributed to triggering the development of a lower level westerly inflow that brought moisture from the continental interior to the mountain. Further observations, such as isotope analysis of snow from the glaciers on Kilimanjaro, would clarify the contribution of different moisture source regions to regional precipitation. In addition, examining a longer time series of TC activity is needed to elucidate the exact storm factors (e.g., number, intensity, or trajectory), and any interactions with other synoptic systems, that trigger or modulate the indirect circulation, as well as the frequency with which they contribute significantly to regional precipitation through either mechanism.

Recent studies have found a positive trend in the number of intense TCs in the SWIO (e.g., Kuleshov et al., 2010; Mavume et al., 2009) consistent with global assessments (e.g., Webster et al., 2005). At the same time, the number making landfall has decreased over the last half century, possibly related to warming of the SWIO as evidenced by a southward displacement of the 26 °C isotherm (Fitchett & Grab, 2014; Mavume et al., 2009). Therefore, future work should examine the contribution that changes in TC activity have made to the regional moistening and drying signals that have an important impact on local populations. An understanding of the contribution of TCs over a longer period will also improve the extraction of climate signals from East Africa's glaciers.

Acknowledgments
This research was funded by the German Research Foundation (DFG) grants MO 2869/1-1, SA 2339/4-1, and MO 2869/3-1, respectively. Support for Northern Icefield AWS measurements was provided by the U.S. National Science Foundation (NSF) and the NOAA Global Climate Observing System. This study was initiated by observations on the mountain by guide Nimrod Charles Kileo ("Timba"), who suggested that a better understanding and prediction of TCs could improve porter safety. The authors gratefully acknowledge the compute resources and support provided by the Erlangen Regional Computing Center (RRZE). Daily mean-simulated atmospheric fields of pressure, temperature, humidity, and winds (originally 1.1 TB in size) are available for download on the Open Science Foundation at doi:10.17605/OSF.IO/3NRST. We thank three anonymous reviewers for their constructive feedback on multiple versions of this manuscript.

References

Ash, K. D., & Matyas, C. J. (2012). The influences of ENSO and the subtropical Indian Ocean Dipole on tropical cyclone trajectories in the southwestern Indian Ocean. *International Journal of Climatology*, *32*(1), 41–56. https://doi.org/10.1002/joc.2249

Astier, N., Plu, M., & Claud, C. (2015). Associations between tropical cyclone activity in the Southwest Indian Ocean and El Niño Southern Oscillation. *Atmospheric Science Letters*, *16*(4), 506–511. https://doi.org/10.1002/asl.589

Banzon, V. F., Reynolds, R. W., Banzon, V. F., & Reynolds, R. W. (2013). Use of WindSat to extend a microwave-based daily optimum interpolation sea surface temperature time series. *Journal of Climate*, *26*(8), 2557–2562. https://doi.org/10.1175/JCLI-D-12-00628.1

Barron, J., Rockström, J., Gichuki, F., & Hatibu, N. (2003). Dry spell analysis and maize yields for two semi-arid locations in east Africa. *Agricultural and Forest Meteorology*, *117*(1-2), 23–37. https://doi.org/10.1016/S0168-1923(03)00037-6

Bessafi, M., & Wheeler, M. C. (2006). Modulation of South Indian Ocean tropical cyclones by the Madden–Julian Oscillation and convectively coupled equatorial waves. *Monthly Weather Review*, *134*(2), 638–656. https://doi.org/10.1175/MWR3087.1

Biswas, M. K., Stark, D., & Carson, L. (2018). GFDL vortex tracker users' guide. Retrieved from https://dtcenter.org/HurrWRF/users/docs/users_guide/standalone_tracker_UG_v3.9a.pdf

Chan, R. Y., Vuille, M., Hardy, D. R., & Bradley, R. S. (2008). Intraseasonal precipitation variability on Kilimanjaro and the East African region and its relationship to the large-scale circulation. *Theoretical and Applied Climatology*, *93*(3–4), 149–165. https://doi.org/10.1007/s00704-007-0338-9

Chang-Seng, D. S., & Jury, M. R. (2010). Tropical cyclones in the SW Indian Ocean. Part 1: Inter-annual variability and statistical prediction. *Meteorology and Atmospheric Physics*, *106*(3-4), 149–162. https://doi.org/10.1007/s00703-009-0055-2

Collier, E., Mölg, T., & Sauter, T. (2018). Recent atmospheric variability at Kibo Summit, Kilimanjaro, and its relation to climate mode activity. *Journal of Climate*. https://doi.org/10.1175/JCLI-D-17-0551.1

Cullen, N. J., Sirguey, P., Mölg, T., & Kaser, G. (2013). A century of ice retreat on Kilimanjaro: The mapping reloaded. *The Cryosphere*, *7*(2), 419–431. https://doi.org/10.5194/tc-7-419-2013

Davies, T. D., Vincent, C. E., & Beresford, A. K. C. (1985). July-August rainfall in West-central Kenya. *Journal of Climatology*, *5*(1), 17–33. https://doi.org/10.1002/joc.3370050103

Davis, C. A. (2018). Resolving tropical cyclone intensity in models. *Geophysical Research Letters*, *45*, 2082–2087. https://doi.org/10.1002/2017GL076966

Dee, D. P., Uppala, S. M., Simmons, A. J., Berrisford, P., Poli, P., Kobayashi, S., et al. (2011). The ERA-Interim reanalysis: Configuration and performance of the data assimilation system. *Quarterly Journal of the Royal Meteorological Society*, *137*(656), 553–597. https://doi.org/10.1002/qj.828

Fitchett, J. M., & Grab, S. W. (2014). A 66-year tropical cyclone record for south-east Africa: Temporal trends in a global context. *International Journal of Climatology*, *34*(13), 3604–3615. https://doi.org/10.1002/joc.3932

Hemp, A. (2005). Climate change-driven forest fires marginalize the impact of ice cap wasting on Kilimanjaro. *Global Change Biology*, *11*(7), 1013–1023. https://doi.org/10.1111/j.1365-2486.2005.00968.x

Hemp, A. (2006). Vegetation of Kilimanjaro: Hidden endemics and missing bamboo. *African Journal of Ecology*, *44*(3), 305–328. https://doi.org/10.1111/j.1365-2028.2006.00679.x

Ho, C.-H., Kim, J.-H., Jeong, J.-H., Kim, H.-S., & Chen, D. (2006). Variation of tropical cyclone activity in the South Indian Ocean: El Niño–Southern Oscillation and Madden-Julian Oscillation effects. *Journal of Geophysical Research*, *111*, D22101. https://doi.org/10.1029/2006JD007289

Huffman, G., Bolvin, D., Nelkin, E., Wolff, D., Adler, R., Gu, G., et al. (2007). The TRMM Multisatellite Precipitation Analysis (TMPA): Quasi-global, multiyear, combined-sensor precipitation estimates at fine scales. *Journal of Hydrometeorology*, *8*(1), 38–55. https://doi.org/10.1175/JHM560.1

Kaser, G., Mölg, T., Cullen, N. J., Hardy, D. R., & Winkler, M. (2010). Is the decline of ice on kilimanjaro unprecedented in the holocene? *Holocene*, *20*(7), 1079–1091. https://doi.org/10.1177/0959683610369498

Kijazi, A. L., & Reason, C. J. C. (2009). Analysis of the 2006 floods over northern Tanzania. *International Journal of Climatology*, *29*(7), 955–970. https://doi.org/10.1002/joc.1846

Klotzbach, P. J. (2014). The Madden-Julian Oscillation's impacts on worldwide tropical cyclone activity. *Journal of Climate*, *27*(6), 2317–2330. https://doi.org/10.1175/JCLI-D-13-00483.1

Kuleshov, Y. (2012). Southern Hemisphere tropical cyclone climatology. *Modern Climatology*, 1–44. Retrieved from. http://digitalcommons.usu.edu/cgi/viewcontent.cgi?article=1000&context=modern_climatology

Kuleshov, Y., Fawcett, R., Qi, L., Trewin, B., Jones, D., McBride, J., & Ramsay, H. (2010). Trends in tropical cyclones in the South Indian Ocean and the South Pacific Ocean. *Journal of Geophysical Research*, *115*, D01101. https://doi.org/10.1029/2009JD012372

Kuleshov, Y., Qi, L., Fawcett, R., & Jones, D. (2008). On tropical cyclone activity in the Southern Hemisphere: Trends and the ENSO connection. *Geophysical Research Letters*, *35*, L14S08. https://doi.org/10.1029/2007GL032983

Madden, R. A., & Julian, P. R. (1994). Observations of the 40–50-day tropical oscillation—A review. *Monthly Weather Review*, *122*(5), 814–837. https://doi.org/10.1175/1520-0493(1994)122<0814:OOTDTO>2.0.CO;2

Matyas, C. J., & Silva, J. A. (2013). Extreme weather and economic well-being in rural Mozambique. *Natural Hazards*, *66*(1), 31–49. https://doi.org/10.1007/s11069-011-0064-6

Mavume, A. F., Rydberg, L., Rouault, M., & Lutjeharms, J. R. E. (2009). Climatology and landfall of tropical cyclones in the South-West Indian Ocean. *Journal of Marine Science*, *8*(1). https://doi.org/10.4314/wiojms.v8i1.56672

Mölg, T., Chiang, J. C. H., Gohm, A., & Cullen, N. J. (2009). Temporal precipitation variability versus altitude on a tropical high mountain: Observations and mesoscale atmospheric modelling. *Quarterly Journal of the Royal Meteorological Society*, *135*(643), 1439–1455. https://doi.org/10.1002/qj.461

Mölg, T., Cullen, N. J., Hardy, D. R., Kaser, G., & Klok, L. (2008). Mass balance of a slope glacier on Kilimanjaro and its sensitivity to climate. *International Journal of Climatology*, *28*(7), 881–892. https://doi.org/10.1002/joc.1589

Mölg, T., Cullen, N. J., Winkler, M., Kaser, G., & Hardy, D. R. (2009). Quantifying climate change in the tropical midtroposphere over East Africa from glacier shrinkage on Kilimanjaro. *Journal of Climate*, *22*(15), 4162–4181.

Mölg, T., & Hardy, D. R. (2004). Ablation and associated energy balance of a horizontal glacier surface on Kilimanjaro. *Journal of Geophysical Research*, *109*, D16104. https://doi.org/10.1029/2003JD004338

Mölg, T., & Kaser, G. (2011). A new approach to resolving climate-cryosphere relations: Downscaling climate dynamics to glacier-scale mass and energy balance without statistical scale linking. *Journal of Geophysical Research*, *116*, D16101. https://doi.org/10.1029/2011JD015669

Moore, G. W. K. (2013). Impact of the high topography of Madagascar on the structure of the Findlater Jet. *Geophysical Research Letters*, *40*, 2367–2372. https://doi.org/10.1002/grl.50399

Mpeta, E. J., & Jury, M. R. (2001). Intra-seasonal convective structure and evolution over tropical East Africa. *Climate Research*, *17*(1), 83–92. https://doi.org/10.3354/cr017083

Mutai, C. C., & Ward, M. N. (2000). East African rainfall and the tropical circulation/convection on intraseasonal to interannual timescales. *Journal of Climate*, *13*(22), 3915–3939. https://doi.org/10.1175/1520-0442(2000)013<3915:EARATT>2.0.CO;2

Pohl, B., & Camberlin, P. (2006). Influence of the Madden-Julian Oscillation on East African rainfall. I: Intraseasonal variability and regional dependency. *Quarterly Journal of the Royal Meteorological Society*, *132*(621), 2521–2539. https://doi.org/10.1256/qj.05.104

Ramsay, H. A., Camargo, S. J., & Kim, D. (2012). Cluster analysis of tropical cyclone tracks in the Southern Hemisphere. *Climate Dynamics*, *39*(3-4), 897–917. https://doi.org/10.1007/s00382-011-1225-8

Reynolds, R. W., Smith, T. M., Liu, C., Chelton, D. B., Casey, K. S., & Schlax, M. G. (2007). Daily high-resolution-blended analyses for sea surface temperature. *Journal of Climate*, *20*(22), 5473–5496. https://doi.org/10.1175/2007JCLI1824.1

Sprenger, M., & Wernli, H. (2015). The LAGRANTO Lagrangian analysis tool version 2.0. *Geoscientific Model Development*, *8*(8), 2569–2586. https://doi.org/10.5194/gmd-8-2569-2015

Sun, L., Semazzi, F. H. M., Giorgi, F., & Ogallo, L. (1999). Application of the NCAR Regional Climate Model to eastern Africa: 2. Simulation of interannual variability of short rains. *Journal of Geophysical Research*, *104*(D6), 6549–6562. https://doi.org/10.1029/1998JD200050

Wallace, J. M., & Hobbs, P. V. (2006). *Atmospheric Science: An Introductory Survey* (2nd ed.). Burlington, MA: Academic Press. https://doi.org/10.1016/C2009-0-00034-8

Wang, C.-C., & Kirshbaum, D. J. (2015). Thermally forced convection over a mountainous tropical island. *Journal of the Atmospheric Sciences*, *72*(6), 2484–2506. https://doi.org/10.1175/JAS-D-14-0325.1

Webster, P. J., Holland, G. J., Curry, J. A., & Chang, H. (2005). Changes in tropical cyclone number, duration, and intensity in a warming environment. *Science*, *309*(5742), 1844–1846. https://doi.org/10.1126/science.1116448

Wheeler, M. C., & Hendon, H. H. (2004). An all-season real-time multivariate MJO index: Development of an index for monitoring and prediction. *Monthly Weather Review*, *132*(8), 1917–1932. https://doi.org/10.1175/1520-0493(2004)132<1917:AARMMI>2.0.CO;2

Whittow, J. B. (1960). Some observations on the snowfall of Ruwenzori. *Journal of Glaciology*, *3*(28), 765–772. https://doi.org/10.1017/S0022143000018074